Rigorous Analysis of a 26-GHz hybrid SIW coupler with Mode Matching Technique

Mohammed A. I. Matar [a] , Gökhan Çınar [a*] and Özge Yanaz Çınar [a]

[a] *Department of Electrical and Electronics Engineering, Faculty of Engineering, Eskişehir Osmangazi University, Turkey.*

Original Research Article

ABSTRACT

In this paper, rigorous Mode-Matching Technique (MMT) with Generalized Scattering Matrix Method (GSMM) is used to analyze novel hybrid SIW coupler operating at 26 GHz for 5G applications. The introduced coupler has an equal-amplitude of about -3 dB besides 90-degree at its forward and coupled output ports with more than 4 GHz bandwidth. In addition to rigorous analysis, full-wave CST simulator is used to optimize coupler structure and the results from MMT and CST are compared and discussed. The coupler structure divided into two symmetrical cascaded parts with each part having multi-port bifurcated sections. Due to symmetrical structure, analyzing one half of the coupler with MMT has been sufficient for full analysis.

1 INTRODUCTION

Directional couplers are passive four-port microwave components [1], which are widely used in many microwave and millimeter-wave systems for splitting or combining power with certain ratios and under specific requirements such as frequencies, bandwidth, and structure dimensions [2, 3, 4, 5]. Directional couplers with equal power and 90° phase-shift output ports are called 90° hybrid couplers [1]. 90° Hybrid couplers can be used in various antenna-feeding networks, radar, power measurements, mixers and other microwave devices [2].

*Corresponding author: Email: gcinar@ogu.edu.tr

Couplers have been incorporated in many microwave systems and applications as mentioned above, therefore, a lot of effort has been put into developing different types, sizes and structures of directional couplers to be used in different applications [6]. Directional couplers can be implemented with many technologies including rectangular waveguides (RCW) and microstrip lines depending on the application needs and structure size. In general, traditional rectangular waveguide couplers have better features than planar couplers regarding to their low insertion losses, high quality factors and power handling. On the other hand, RCW's are difficult to manufacture and they are not easy to integrate into planar microwave systems [7].

For broadband high frequency applications, dimensions of the rectangular waveguide become too small and difficult to implement even with advanced fabrication techniques, therefore,Substrate Integra-ted Waveguide (SIW) technology has been introduced as a suitable way to implement structures such as in [2, 8, 7, 9, 14, 10, 11, 12]. SIW structures have common advantages with printed circuits such as low cost, small size and planar integration. Moreover, SIW technology shares with rectangular waveguides (RCW) most of its properties like low losses and high Q-factors as it is covered by metal surfaces on both sides of the substrate with metal vias integrated within it to work as vertical walls [13].

In the last decade, SIW couplers are preferred more often in high frequency applications because of their above-mentioned properties. In [14], a wideband 90° hybrid SIW coupler having a wide operating bandwidth with obtained fractional bandwidth (FBW) of about 28.5% at 33.5 GHz is presented. Since this coupler operates in the millimeter-wave range and it is a multi-hole type of a coupler, using SIW technique allows its fabrication to be much easier compared to other techniques. Although the compact size, broadband SIW cruciform coupler design (cruciform couplers are usually described as 90° hybrid couplers [15]) introduced in [6] operates in the same frequency range, it has a narrower fractional bandwidth of 18%. While the forward and coupling signals amplitudes must be –3 dB ideally in hybrid couplers, the results in [6] indicate values between -4 dB

and –6 dB due to the losses in the microstrip line feeder. Hybrid SIW coplanar waveguide (CPW) structure coupler is presented in [11] with a fractional bandwidth of about 30% (which is a good result when a planar feeder is used) beside its 90° phase shift between the output ports. The reason of using the grounded coplanar waveguide (GCPW) in the design is to make coupling of the vertical electric fields in SIW with the horizontal electric fields in CPW simpler. Although, results obtained from analyzing SIW coupler structures with commercial full-wave analysis softwares such as CST and HFSS [16] are satisfying, parametric studies and optimization of the designs have large time consumption and they need much memory. Mode Matching Technique, especially with the Generalized Scattering Matrix Method (GSMM) is proven to be very useful and powerful in microwave designs relying upon waveguide structures having discontinuities either physically or geometrically [17]. For example, the paper in [18] considered MMT with GSMM in the analyses of some sectoral waveguide mode converters. In [19], a simple and straightforward MMT approach is presented to analyze SIW coupler with circular vias, which are converted into square shape vias with some restrictions in order to define the structure discontinuities easily. Recently, there have been many other works where MMT with GSMM is applied to several SIW components which introduce fast, exact and robust analyses [20, 21, 19, 22, 23, 24].

This research paper introduces the rigorous MMT procedure to analyze a hybrid SIW coupler operating at 26 GHz for 5G applications. Accurate and fast results are obtained by using MMT, which include the consideration of symmetrical multi-port cascading GSMM. The hybrid coupler is designed to has an equal-amplitude of -3dB besides 90° phase shift at its forward and coupled output ports with more than 4 GHz bandwidth. In cascading analysis for the SIW structure, square vias are assumed as the discontinuities and when connecting the 2×2 part to 3×3 part, we considered the phase shift in the signal due to the fixed length of the common region. The proposed coupler is also optimized with full-wave solver CST and the results regarding the S-parameters and phase shifts are compared with the ones obtained via MMT.

2 DESIGN AND ANALYSIS

2.1 SIW Structure

SIW structure in Fig. 1. is very similar to a dielectric filled waveguide (DFW) structure as it is formed of two rows of cylindrical vias (waveguide walls) between metal cover plates, which are separated by a dielectric substrate. So, the E-field distribution in SIW is quite similar to the one in DFW [25].
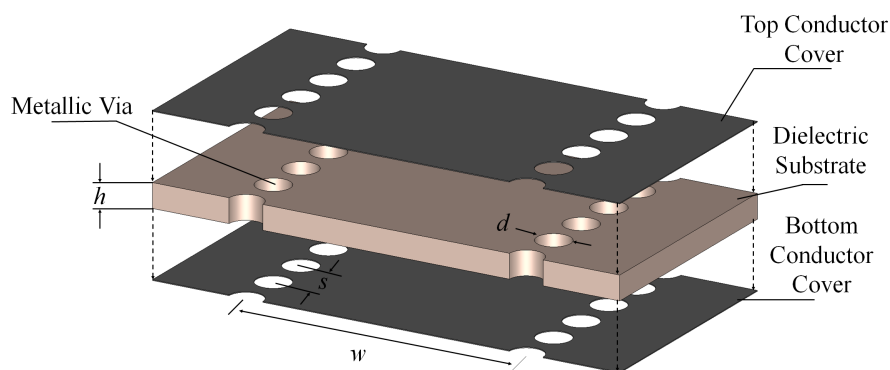

Fig. 1. SIW configuration

The main three SIW design parameters are; SIW width w, metallic via diameter d and the pitch s. In order to avoid any leakage from the structure, these parameters must be calculated using below formulas [7, 25]:
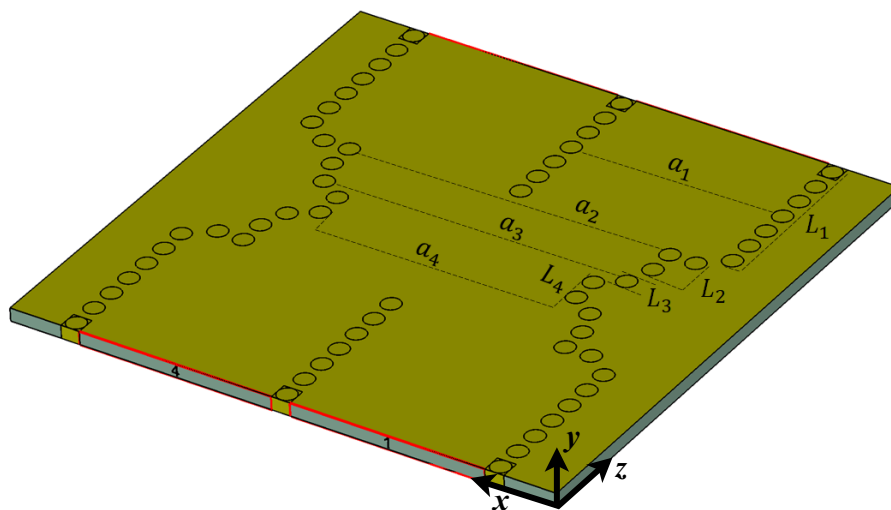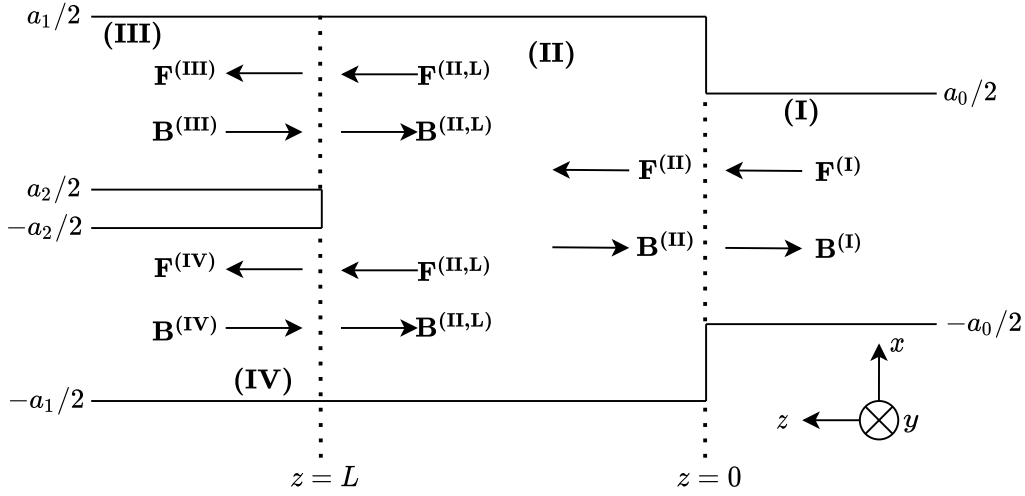

Fig. 2. SIW 3D coupler structure

$$w_{eff} = w - \frac{d^2}{0.95 \times s} \tag{2.1}$$

$$d < \frac{\lambda_g}{5}, \quad s \leq 2d \tag{2.2}$$

Fig. 3. Geometrical model for mode-matching analysis.

$$\lambda_g = \frac{2\pi}{\sqrt{\frac{\varepsilon_r (2\pi f)^2}{c^2} \left(\frac{\pi}{w}\right)}} \tag{2.3}$$

where, f is the frequency, λ_g is the guided wavelength and c is the speed of light. In the next subsection, SIW technology will be implemented to design hybrid SIW coupler with $d = 0.72$ mm and $s = 1.0015$ mm.

2.2 SIW Directional Coupler Design

Fig.2. shows the designed structure of a 3-dB hybrid SIW coupler with its symmetrical dimensions. RT Duroid 5880 substrate with a relative permittivity of ϵ_r=2.2 , tangent loss of $\tan \delta$=0.0009 and substrate height of 508μm is used to implement this coupler. Figure also illustrates the coupler parameter values for the frequency range of 23 GHz to 27 GHz. The designed coupler is symmetric around x-axis and z-axis, which is the directions of wave propagation. Since the coupler structure is symmetric around z-axis, analyzing one half of the structure with MMT is enough for full GSMM analysis.

Table. 1. SIW Coupler Parameters

Parameter	mm
a_1	7.47
a_2	11.75
a_3	11.03
a_4	9.22
L_1	6.729
L_2	2.1
L_3	0.589
L_4	1.721

2.3 Mode-Matching Analysis

The designed coupler is analyzed rigorously with Mode Matching Technique by considering the first half of it as a single structure and then cascading this half with its mirror image which becomes enough to complete the structure. The geometrical model of the problem is presented in Fig. . X denoting the regions I, II, III and IV and $k_{zm}^{(X)}$ being the wavenumber of the m-th mode propagating in the relevant region as:

$$
k_{zm}^{(X)} = \begin{cases} \sqrt{\omega^2 \mu \epsilon - \left(\frac{m\pi}{b^{(X)}}\right)^2} & : \text{propagating mode} \\ -\mathrm{j}\sqrt{\left(\frac{m\pi}{b^{(X)}}\right)^2 - \omega^2 \mu \epsilon} & : \text{evanescent mode} \end{cases} ,
\tag{2.4}
$$

the fields in their relevant regions are expressed in terms of normaized modes as

$$
E_y^{(X)} = \sum_{m=1}^{\infty} G_m^{(X)} \sin\left[\frac{m\pi(x + d^{(X)})}{b^{(X)}}\right] \times \left[F_m^{(X)} \mathrm{e}^{-\mathrm{j}k_{zm}^{(X)}z} + B_m^{(X)} \mathrm{e}^{\mathrm{j}k_{zm}^{(X)}z}\right]
\tag{2.5}
$$

and

$$
H_x^{(X)} = -\sum_{m=1}^{\infty} G_m^{(X)} Y_m^{(X)} \sin\left[\frac{m\pi(x + d^{(X)})}{b^{(X)}}\right] \times \left[F_m^{(X)} \mathrm{e}^{-\mathrm{j}k_{zm}^{(X)}z} - B_m^{(X)} \mathrm{e}^{\mathrm{j}k_{zm}^{(X)}z}\right]
\tag{2.6}
$$

with

$$
Y_m^{(X)} = \frac{k_{zm}^{(X)}}{\omega\mu},
\tag{2.7}
$$

$$
G_m^{(X)} = 2\sqrt{\frac{\omega\mu}{b^{(X)} h k_{zm}^{(X)}}},
\tag{2.8}
$$

$$
d^{(X)} = \begin{cases} a_0/2 & : X = I \\ a_1/2 & : X = II \\ -a_2/2 & : X = III \\ a_1/2 & : X = IV \end{cases}
\tag{2.9}
$$

and

$$
b^{(X)} = \begin{cases} a_0 & : X = I \\ a_1 & : X = II \\ (a_1 - a_2)/2 & : X = III \\ (a_1 + a_2)/2 & : X = IV \end{cases}
\tag{2.10}
$$

These modes are matched at the interfaces of the regions by considering the tangential components of the electric fields and the magnetic fields are continuous. The continuity relations at $z = 0$ for the system formed by regions I and II are

$$
E_y^{(II)} = \begin{cases} E_y^{(I)} & : -a_0/2 \leq x \leq a_0/2 \\ 0 & : \text{elsewhere} \end{cases}
\tag{2.11}
$$

and

$$
H_x^{(I)} = H_x^{(II)}, \quad -a_0/2 \leq x \leq a_0/2.
\tag{2.12}
$$

Applying these conditions to the fields in their relevant regions, we obtain

$$
\begin{bmatrix} \mathbf{B^{(I)}} \\ \mathbf{F^{(II)}} \end{bmatrix} = \begin{bmatrix} \mathbf{S_{11}^{(0)}} & \mathbf{S_{12}^{(0)}} \\ \mathbf{S_{21}^{(0)}} & \mathbf{S_{22}^{(0)}} \end{bmatrix} \begin{bmatrix} \mathbf{F^{(I)}} \\ \mathbf{B^{(II)}} \end{bmatrix}
\tag{2.13}
$$

with

$$
\mathbf{S_{11}^{(0)}} = \left(\mathbf{I} + \mathbf{L_H^{(0)}} \mathbf{L_E^{(0)}}\right)^{-1} \left(\mathbf{I} - \mathbf{L_H^{(0)}} \mathbf{L_E^{(0)}}\right),
\tag{2.14}
$$

$$\mathbf{S}_{12}^{(0)} = 2\left(\mathbf{I} + \mathbf{L}_{H}^{(0)}\mathbf{L}_{E}^{(0)}\right)^{-1}\mathbf{L}_{H}^{(0)}, \tag{2.15}$$

$$\mathbf{S}_{21}^{(0)} = 2\left(\mathbf{I} + \mathbf{L}_{E}^{(0)}\mathbf{L}_{H}^{(0)}\right)^{-1}\mathbf{L}_{E}^{(0)} = \mathbf{L}_{E}^{(0)}\left(\mathbf{I} + \mathbf{S}_{11}^{(0)}\right) \tag{2.16}$$

and

$$\mathbf{S}_{22}^{(0)} = \left(\mathbf{I} + \mathbf{L}_{E}^{(0)}\mathbf{L}_{H}^{(0)}\right)^{-1}\left(\mathbf{L}_{E}^{(0)}\mathbf{L}_{H}^{(0)} - \mathbf{I}\right) = \left(\mathbf{L}_{E}^{(0)}\mathbf{S}_{12}^{(0)} - \mathbf{I}\right) \tag{2.17}$$

Here, $\mathbf{L_E}$ and $\mathbf{L_H}$ stand for the integrals

$$\left(L_{E}^{(0)}\right)_{mn} = 2\sqrt{\frac{k_{zm}^{(II)}}{a_0 a_1 k_{zn}^{(I)}}} \int_{-\frac{a_0}{2}}^{\frac{a_0}{2}} \sin\left(\frac{m\pi(x + a_1/2)}{a_1}\right) \times \sin\left(\frac{n\pi(x + a_0/2)}{a_0}\right)\mathrm{d}x \tag{2.18}$$

and

$$\left(L_{H}^{(0)}\right)_{mn} = \left(L_{E}^{(0)}\right)_{nm} \tag{2.19}$$

while $\mathbf{I}$ being the unit matrix. Similarly, for the system formed by the regions II, III and IV, the continuity relations at $z = L$ are

$$E_y^{(II)} = \begin{cases} E_y^{(III)} & : a_2/2 \leq x \leq a_1/2 \\ 0 & : -a_2/2 \leq x \leq a_1/2 \\ E_y^{(IV)} & : -a_1/2 \leq x \leq -a_2/2 \end{cases}, \tag{2.20}$$

$$H_x^{(III)} = H_x^{(II)}, \;\; a_2/2 \leq x \leq a_1/2 \tag{2.21}$$

and

$$H_x^{(IV)} = H_x^{(II)}, \;\; -a_1/2 \leq x \leq -a_2/2. \tag{2.22}$$

Substituting the fields in their relevant regions into the above conditions yields

$$\begin{bmatrix} \mathbf{B^{(II,L)}} \\ \mathbf{F^{(III)}} \\ \mathbf{F^{(IV)}} \end{bmatrix} = \begin{bmatrix} \mathbf{S}_{11}^{(L)} & \mathbf{S}_{12}^{(L)} & \mathbf{S}_{13}^{(L)} \\ \mathbf{S}_{21}^{(L)} & \mathbf{S}_{22}^{(L)} & \mathbf{S}_{23}^{(L)} \\ \mathbf{S}_{31}^{(L)} & \mathbf{S}_{32}^{(L)} & \mathbf{S}_{33}^{(L)} \end{bmatrix} \begin{bmatrix} \mathbf{F^{(II,L)}} \\ \mathbf{B^{(III)}} \\ \mathbf{B^{(IV)}} \end{bmatrix} \tag{2.23}$$

where

$$\mathbf{S}_{11}^{(L)} = \left(\mathbf{I} + \mathbf{L}_{E1}^{(L)}\mathbf{L}_{H1}^{(L)} + \mathbf{L}_{E2}^{(L)}\mathbf{L}_{H2}^{(L)}\right)^{-1}$$
$$\times \left(\mathbf{L}_{E1}^{(L)}\mathbf{L}_{H1}^{(L)} + \mathbf{L}_{E2}^{(L)}\mathbf{L}_{H2}^{(L)} - \mathbf{I}\right) \tag{2.24}$$

$$\mathbf{S}_{12}^{(L)} = 2\left(\mathbf{I} + \mathbf{L}_{E1}^{(L)}\mathbf{L}_{H1}^{(L)} + \mathbf{L}_{E2}^{(L)}\mathbf{L}_{H2}^{(L)}\right)^{-1}\mathbf{L}_{E1}^{(L)} \tag{2.25}$$

$$\mathbf{S}_{13}^{(L)} = 2\left(\mathbf{I} + \mathbf{L}_{E1}^{(L)}\mathbf{L}_{H1}^{(L)} + \mathbf{L}_{E2}^{(L)}\mathbf{L}_{H2}^{(L)}\right)^{-1}\mathbf{L}_{E2}^{(L)} \tag{2.26}$$

$$\mathbf{S}_{21}^{(L)} = \left(\mathbf{L}_{H1}^{(L)} - \mathbf{L}_{H1}^{(L)}\mathbf{S}_{11}^{(L)}\right) \tag{2.27}$$

$$\mathbf{S}_{22}^{(L)} = \left(\mathbf{I} - \mathbf{L}_{H1}^{(L)}\mathbf{S}_{12}^{(L)}\right) \tag{2.28}$$

$$\mathbf{S}_{23}^{(L)} = -\mathbf{L}_{H1}^{(L)}\mathbf{S}_{13}^{(L)} \tag{2.29}$$

$$\mathbf{S}_{31}^{(L)} = \left(\mathbf{L}_{H2}^{(L)} - \mathbf{L}_{H2}^{(L)}\mathbf{S}_{11}^{(L)}\right) \tag{2.30}$$

$$\mathbf{S}_{32}^{(L)} = -\mathbf{L}_{H2}^{(L)}\mathbf{S}_{12}^{(L)} \tag{2.31}$$

and

$$\mathbf{S}_{33}^{(L)} = \left(\mathbf{I} - \mathbf{L}_{H2}^{(L)}\mathbf{S}_{13}^{(L)}\right) \tag{2.32}$$

with

$$\left(L_{E1}^{(L)}\right)_{mn} = 2\sqrt{\frac{2k_{zm}^{(II)}}{a_1(a_1-a_2)k_{zn}^{(III)}}}\int_{\frac{a_2}{2}}^{\frac{a_1}{2}}\sin\left(\frac{m\pi\left(x+\frac{a_1}{2}\right)}{a_1}\right)$$

$$\times \sin\left(\frac{n\pi\left(x-\frac{a_2}{2}\right)}{\frac{a_1}{2}-\frac{a_2}{2}}\right)\mathrm{d}x = \left(L_{H1}^{(L)}\right)_{nm} \tag{2.33}$$

and

$$\left(L_{E2}^{(L)}\right)_{mn} = 2\sqrt{\frac{2k_{zm}^{(I)}}{a_1(a_1-a_2)k_{zn}^{(IV)}}}\int_{-\frac{a_1}{2}}^{-\frac{a_2}{2}}\sin\left(\frac{m\pi\left(x+\frac{a_1}{2}\right)}{a_1}\right)$$

$$\times \sin\left(\frac{n\pi\left(x+\frac{a_1}{2}\right)}{\frac{a_1}{2}-\frac{a_2}{2}}\right) = \left(L_{H2}^{(L)}\right)_{nm}. \tag{2.34}$$

In order to apply generalized scattering matrix method when cascading this 3×3 system to the 2×2 system as it is presented in Figure , the relations

$$\mathbf{F^{(I,L)}} = \mathbf{DF^{(I)}} \tag{2.35}$$

$$\mathbf{B^{(I)}} = \mathbf{DB^{(I,L)}} \tag{2.36}$$

with

$$\mathbf{D} = \mathrm{diag}\left\{\mathrm{e}^{-\mathrm{j}k_{zm}^{(I)}L}\right\} \tag{2.37}$$

are considered. Finally by the help of Generalized Scattering Matrix Method,

$$\begin{bmatrix}\mathbf{B^{(I)}}\\\mathbf{F^{(III)}}\\\mathbf{F^{(IV)}}\end{bmatrix} = \begin{bmatrix}\mathbf{S_{11}}&\mathbf{S_{12}}&\mathbf{S_{13}}\\\mathbf{S_{21}}&\mathbf{S_{22}}&\mathbf{S_{23}}\\\mathbf{S_{31}}&\mathbf{S_{32}}&\mathbf{S_{33}}\end{bmatrix}\begin{bmatrix}\mathbf{F^{(I)}}\\\mathbf{B^{(III)}}\\\mathbf{B^{(IV)}}\end{bmatrix} \tag{2.38}$$

is determined with

$$\mathbf{S_{11}} = \mathbf{S_{11}^{(0)}} + \mathbf{S_{12}^{(0)}DUS_{11}^{(L)}DS_{21}^{(0)}} \tag{2.39}$$

$$\mathbf{S_{12}} = \mathbf{S_{12}^{(0)}DUS_{12}^{(L)}} \tag{2.40}$$

$$\mathbf{S_{13}} = \mathbf{S_{12}^{(0)}DUS_{13}^{(L)}} \tag{2.41}$$

$$\mathbf{S_{21}} = \mathbf{S_{21}^{(L)}DVS_{21}^{(0)}} \tag{2.42}$$

$$\mathbf{S_{22}} = \mathbf{S_{21}^{(L)}DVS_{22}^{(0)}DS_{12}^{(L)}} + \mathbf{S_{22}^{(L)}} \tag{2.43}$$

$$\mathbf{S_{23}} = \mathbf{S_{21}^{(L)}DVS_{22}^{(0)}DS_{13}^{(L)}} + \mathbf{S_{23}^{(L)}} \tag{2.44}$$

$$\mathbf{S_{31}} = \mathbf{S_{31}^{(L)}DVS_{21}^{(0)}} \tag{2.45}$$

$$\mathbf{S_{32}} = \mathbf{S_{31}^{(L)}DVS_{22}^{(0)}DS_{12}^{(L)}} + \mathbf{S_{32}^{(L)}} \tag{2.46}$$

and

$$\mathbf{S_{33}} = \mathbf{S_{31}^{(L)}DVS_{22}^{(0)}DS_{13}^{(L)}} + \mathbf{S_{33}^{(L)}} \tag{2.47}$$

Here the matrices $\mathbf{U}$ and $\mathbf{V}$ stand for

$$\mathbf{U} = \left(\mathbf{I} - \mathbf{S_{11}^{(L)}DS_{22}^{(0)}D}\right)^{-1} \tag{2.48}$$

and

$$\mathbf{V} = \left(\mathbf{I} - \mathbf{S_{22}^{(0)}DS_{11}^{(L)}D}\right)^{-1}, \tag{2.49}$$

respectively. Having formulated one half of the coupler design, it can easily be applied to the other half which allows the full geometry rigorously analyzed by MMT.
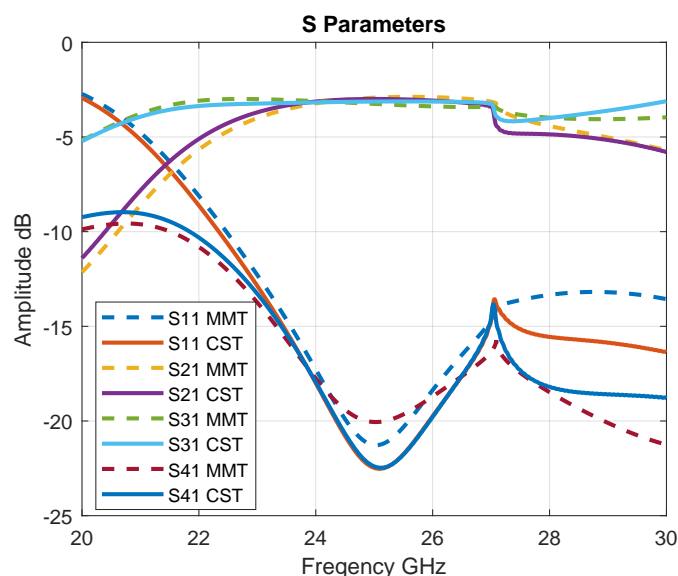
S Parameters

Fig.4. SIW coupler frequency response with MMT and CST.

3 RESULTS AND DISCUSSION

Fig. 2.3 illustrates the frequency response of the designed SIW coupler when dimensions in Table are used. The usage of RT Duroid 5880 substrate which have low relative permittivity of 2.2 decreases the substrate losses compared with other substrates with higher relative permittivity. Figure 2.3 also shows that the designed coupler has a fractional bandwidth (FBW) of about 16% with respect to 25 GHz as center frequency. FBW is calculated by considering equal amplitude (-3 dB) and 90 degree phase shift of coupled and forwarded output ports, namely port 2 and port 3, respectively. The designed coupler also introduces high isolation between the feeding port (port 1) and port 4 with more than 20 dB. In this design, as the length L_4 increases, the amplitude output at port 3 increases, and the amplitude output at port 2 decreases, so that it can be observed that L_4 with output widths can control the output amplitudes.

The observed discontinuity near 27 GHz in the frequency response emerges due to the appearance of a higher-order mode which is TE_{20} in the coupler structure . In fabrication process, a matched microstrip-line-to-SIW transaction can be used to feed the designed coupler. Although there are some structure approximations (such as square vias and zero length region), good agreement between MMT and CST is achieved.

The truncation number for MMT analysis is chosen as 45. Higher truncation number means higher accuracy, however for truncation numbers above 25, the differences in the results are negligible.Phase shift of 90 ± 5 degrees is achieved between forward and coupled output ports as can be seen in Figure 2.3, which also presents a good agreement between CST and MMT results. The phase shift property allows this coupler to be a part of beamforming antenna feeding networks. The electrical field distribution at 26 GHz is presented in Figure 2.3. In this Figure, it can be seen that the input signal from port 1 interacts with metallic vias as if they are conductive walls in rectangular waveguides, and is coupled equally to port 2 and port 3 with good isolation on port 4.
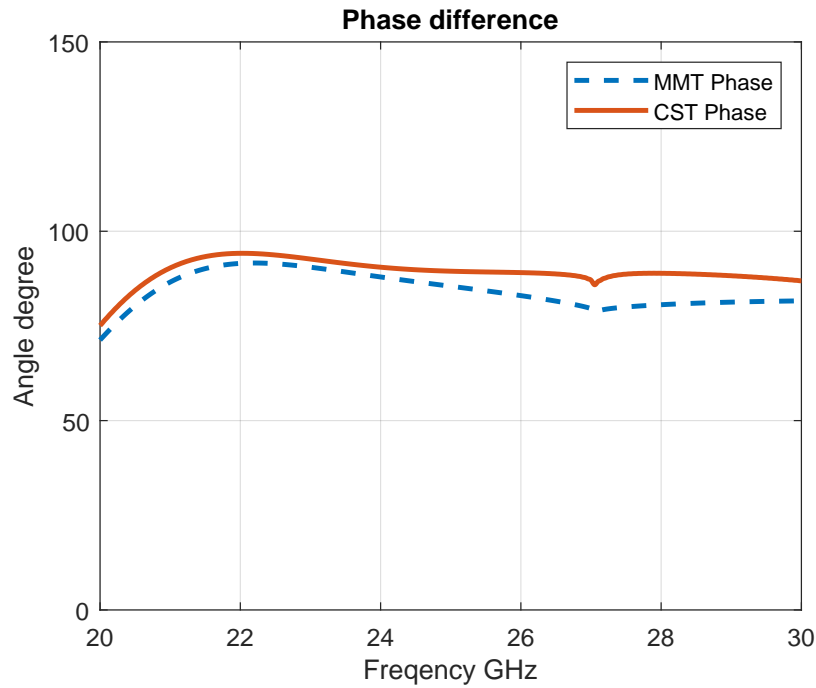
Phase difference

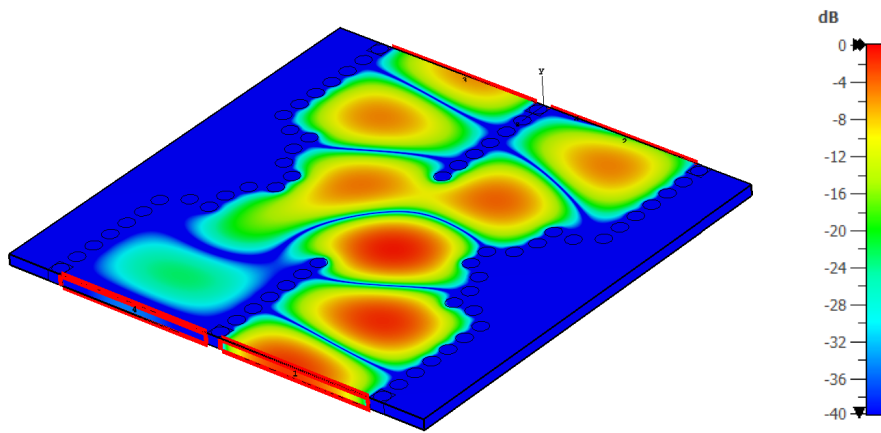**Fig.5. Output ports phase difference obtained by MMT and CST.**

Fig. 6. E-Field distribution of the analyzed coupler

4 CONCLUSION

Mode-Matching Technique (MMT) analysis with Generalized Scattering Matrix Method (GSMM) of SIW hybrid coupler is presented in this paper. Multi-port cascading approach presented and discussed to analyze and formulate full coupler scattering matrix. The suggested coupler is analyzed Using MMT Matlab code with 45 as a truncation number and simulated with full-wave solver CST .The designed coupler presents -3 dB equal-amplitude output ports

and more than 20 dB of port isolation with about 90-degree phase shift. Despite some structure approximations in the MMT procedure, good agreement is determined between the S-parameter results obtained by the rigorous analysis with MMT and those from full-wave solver CST.

COMPETING INTERESTS

Authors have declared that no competing interests exist.

REFERENCES

[1] Pozar DM. Microwave engineering. John wiley sons; 2011.

[2] Ahmad BH, Sabri SS, Othman AR. Design of a compact X-Band substrate integrated waveguide directional coupler. International Journal of Engineering Technology. 2013;5(2):1905-11.

[3] Jung J, Lee G, Song JI. A directional coupler with suppressed Tx leakage for UHF RFID reader applications. Journal of Electromagnetic Waves and Applications. 2016;30(2):225-31.
Available: https://doi.org/10.1080/09205071.2015.1105154

[4] Lin G, Yin X, Ren S, Wang Z, Zhi Y, He T. Compact and broadband directional coupler for high power applications. Journal of Electromagnetic Waves and Applications. 2021;35(15):1980-6.
Available: https://doi.org/10.1080/09205071.2021.1926339

[5] Hadj Aissa Fekhar Y, Salah-Belkhodja F, Vincent D, Bronchalo E, Tebboune W, Naoum R. Microwave non-reciprocal coplanar directional coupler based on ferrite materials. Journal of Electromagnetic Waves and Applications. 2020;34(5):623-33.

[6] Guan DF, Qian ZP, Zhang YS, Cai Y. Hybrid SIW-GCPW cruciform directional coupler. Frequenz. 2014;68(1-2):39-42.

[7] Boulesbaa M, Djerafi T, Bouchekhlal A, Mekimah B. Design of a Directional Coupler Based on SIW Technology for X Band Applications. In2020 1st International Conference on Communications, Control Systems and Signal Processing (CCSSP).2020;85-89. IEEE.

[8] Mahant K, Mewada H. A novel substrate integrated waveguide (SIW) based highly selective filter for radar applications. Journal of Electromagnetic Waves and Applications. 2019;33(13):1718-25.

[9] Tiwari NK, Singh SP, Akhtar MJ. Novel substrate integrated waveguide cavity-based unified multiband permittivity and permeability estimation approach. Journal of Electromagnetic Waves and Applications. 2020;34(18):2499-513.

[10] Sun PF, Shen W, Wu L, Qian R, Sun XW. Compact substrate integrated waveguide transversal filter with mixed source–load coupling. Journal of Electromagnetic Waves and Applications. 2016;30(2):167-74.

[11] Guan DF, Qian ZP, Zhang YS, Cai Y. A hybrid SIW and GCPW guided-wave structure coupler. IEEE microwave and wireless components letters. 2014;24(8):518-20.

[12] Rana B, Parui SK. H-plane horn antenna using corrugated substrate integrated waveguide. Journal of ElEctromagnEtic WavEs and applications. 2016 ;30(14):1869-76.

[13] Nasri A, Zairi H, Gharsallah A. Design of a novel structure SIW $90°$ coupler. American Journal of Applied Sciences. 2016; 13(3):276—280.

[14] Tavakoli MJ, Mallahzadeh AR. Wideband directional coupler for millimeter wave application based on substrate integrated waveguide. Emerging Science Journal. 2018;2(2):93-9.

[15] Mansouri Z, Kishihara M, Zarrabi FB, Geran F, Hesarak T. Broadband half mode substrate integrated waveguide cruciform coupler. InThe Second Iranian Conference on Engineering Electromagnetics (ICEEM 2014). 2014;595-599.

[16] Kordiboroujeni Z, Bornemann J. Design of substrate integrated waveguide

components using mode-matching techniques. In2015 IEEE MTT-S International Conference on Numerical Electromagnetic and Multiphysics Modeling and Optimization (NEMO). 2015;1-3. IEEE.

[17] Matar MA, Cınar G, Cınar OY. Analysis of SIW Crossover for 5G Beamforming Network Applications. International Journal of Engineering Technology. 2022;11(1):50-8.

[18] Kumar V, Dwivedi S, Jain PK. Mode-matching analysis for characterization of the sectoral waveguide mode converters. Microwave and Optical Technology Letters. 2019;61(11):2619-27.

[19] Kordiboroujeni Z, Bornemann J, Sieverding T. Mode-matching design of substrate-integrated waveguide couplers. In2012 Asia-Pacific Symposium on Electromagnetic Compatibility. 2012;701-704). IEEE.

[20] Bornemann J, Taringou F. Substrate-integrated waveguide filter design using mode-matching techniques. In2011 41st European Microwave Conference.2011;l1-4). IEEE.

[21] Kordiboroujeni Z, Taringou F, Bornemann J. Efficient mode-matching design of substrate-integrated waveguide filters. In2012 42nd European Microwave Conference. 2012;253-256. IEEE.

[22] Kordiboroujeni Z, Bornemann J. Mode matching design of substrate integrated waveguide diplexers. In2013 IEEE MTT-S International Microwave Symposium Digest (MTT).2013;1-3). IEEE.

[23] Schorer J, Bornemann J. A mode-matching technique for the analysis of waveguide-on-substrate components. In2015 IEEE MTT-S International Conference on Numerical Electromagnetic and Multiphysics Modeling and Optimization (NEMO). 2015;1-3). IEEE.

[24] Bornemann J, Hesari SS. Scattering matrix subtraction technique for mode-matching analysis of substrate integrated waveguide junctions. In2017 IEEE MTT-S International Conference on Numerical Electromagnetic and Multiphysics Modeling and Optimization for RF, Microwave, and Terahertz Applications (NEMO). 2017;1-3. IEEE.

[25] Wang J, Ling T. Novel broadband design of SIW directional coupler. The Journal of Engineering. 2019;2019(20):6633-6.